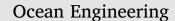
Contents lists available at ScienceDirect





journal homepage: www.elsevier.com/locate/oceaneng

Gas flows and losses inside high-speed ventilated supercavitating flows



OCEAN

Key Laboratory of Hydrodynamics (Ministry of Education), Department of Engineering Mechanics, Shanghai Jiao Tong University, Shanghai, 200240, China

ARTICLE INFO

Keywords: Ventilated supercavitating flows Multi-fluid model Velocity distribution Gas loss

ABSTRACT

Wang Zou^{*}, Leiping Xue, Benlong Wang, Xintao Xiang

Internal gaseous velocity distribution and gas loss are significant and interconnected mechanisms of ventilated supercavitating flows. Considering gas-vapor-water momentum interactions and vapor-water mass transport, a multi-fluid model has been established for high speed ventilated supercavitating flows. Based on the model, the velocity distributions in the longitudinal and cross-sectional planes are analyzed to clearly reveal the gas loss mechanism for the flows around cavitator and body. For the former, two vortex cores are formed in the longitudinal plane and are symmetrically distributed about the longitudinal axis. Most inner regions in the cavity cross section are occupied by circulation flows; when passing the vortex center, the direction of the velocity changes, and the component in the radial direction increases. The gas departs to wake flows in the outermost regions close to the section boundary. The velocity distribution law in a characteristic cross section through vortex cores does not depend on cavitation number. For the supercavitating body, there is a similar entrainment mechanism, and multiple axisymmetrical vortices may be distributed inside the cavity. The velocity distributions go through turning points in the characteristic sections covering the inner body, whereas the distribution has a monotonic trend in the section without the inner body near the body tail. The tail pressure gradient influences velocity differences in the inner regions of the sections close to the supercavity tails at different cavitation numbers. Using computations of the flows at different Reynolds and cavitation numbers, the dependence of gas loss on Reynolds number is also presented.

1. Introduction

Improved theories and technologies of ventilated supercavitating flows will accelerate the development of underwater high-speed vehicles. Subsequent to observations of drag reduction due to supercavitation, significant advances have been made in understanding the formation, stability and hydrodynamic forces of supercavitating flows (Stinebring et al., 2002; Kirschner et al., 2001; Lindau and Kunz, 2004; Lu et al., 2007; Wei et al., 2007; Zou and Liu, 2015a). Only a few studies have focused on internal flow structures of ventilated supercavitating flows (Kinzel et al., 2009; Savchenko and Savchenko, 2012). Flow velocity distribution inside high-speed supercavity remains to be studied further, and those distribution laws determine the gas loss mechanisms closely related to the stability (Paryshev, 2003) and control (Zou and Liu, 2015b) of flows around vehicles. By and large, there are two gas loss regimes, i.e., two vortex tubes and toroidal vortices, which were experimentally well observed by Epstein (1973), and research developments were discussed by Zou and Liu (2015b). Although two vortex tubes are often found in water tunnels with small Froude numbers (Kawakami and Arndt, 2011), the toroidal vortex mode usually dominates gases departing from ventilated supercavities at high Froude numbers caused by high speeds in unbounded flows. The transition modes between the two mechanisms were further revealed by Karn et al. (2015, 2016) using water tunnel experiments. Epstein's entrainment model has been widely accepted for vortex tubes (Epstein, 1961). In the case of the toroidal vortex mode focused on here, a reentrant jet occurs in the supercavity's tail under the action of the adverse pressure gradient, where the gas-liquid mediums collide to form foam structures. Some of the foams fill the cavity end, and the others leave with non-condensable gas along the cavity wall in the form of toroidal vortices (Wang et al., 2015). Logvinovich (1969) modeled this gas loss using a dimensional analysis method when gravity effect is not considered. The model is suitable for the case that cavitation number without the action of ventilation approached natural one. Further, the gas entrainment theoretical assumption made by Spurk (2002a) has been experimentally confirmed (Savchenko and Savchenko, 2012). Based on the homogenous multiphase model, a local gas entrainment rate was defined by Kinzel et al. (2009) to show internal gaseous streamlines for ventilated supercavitating flows, and a similar gas loss mode also applies to the main structure of the supercavity with two vortex tubes. The escaped gas finally occupies the entirety of the cross sections of the vortex tubes.

https://doi.org/10.1016/j.oceaneng.2018.06.030 Received 31 October 2017; Received in revised form 5 February 2018; Accepted 9 June 2018 0029-8018/ © 2018 Elsevier Ltd. All rights reserved.

^{*} Corresponding author. School of Naval Architecture, Ocean & Civil Engineering, Shanghai Jiao Tong University, Shanghai, China. *E-mail address*: hopingzou@sjtu.edu.cn (W. Zou).

Considering momentum interactions and mass transport between phases, the gas-vapor-water multi-fluid model, which is based on the theory for nonhomogeneous multiphase flows, is established for ventilated supercavitating flows in the CFD solver CFX. Because each phase is respectively solved in the model, ventilated supercavitating flows at high speeds can be simulated to directly determine the internal gaseous velocity field. The velocity distributions were analyzed to clearly reveal the gas loss mechanisms in the longitudinal and cross-sectional planes. By simulating the flows at different Reynolds and cavitation numbers, the dependence of gas loss on Reynolds number was obtained. The analyses of the internal velocity field and gas loss law aid in deepening the understanding of the gas-leakage mechanism for the dynamics model of the maneuvering ventilated supercavity (Zou et al., 2016) and can provide greater detail for models and methods used to control supercavitating flows (Yu et al., 2013; Zou and Liu, 2015b).

2. Multi-fluid model and numerical method

In a ventilated supercavitating flow, there is an obvious gas-liquid phase interface, except in the tail closure region. The flows inside and outside the cavity differ fundamentally and interact among each other (Yu et al., 2010; Xiang et al., 2011). Flow interactions in different phases are inevitable and can be considered sequentially (Kunz et al., 2003), such that the two-fluid model is suitable for describing ventilated supercavitating flows (Yu et al., 2012) alongside microbubble boundary layer flows to achieve drag reduction using bubble dynamics and the mass transport mechanism (Kunz et al., 2007). However, flow parameters may be more complex in unsteady flows, and natural cavitation can occur when liquid pressures drop below saturated vapor pressure. Taking into further account the vaporization effect in high-speed flows, a gas-vapor-water multi-fluid model is developed for the flows here.

2.1. Governing equations

Based on the theory of nonhomogeneous multiphase flows, the governing equations consist of the continuity and momentum equations of each phase and the volume conservation and pressure constraint equations if supercavitating flows are considered to be approximately isothermal. Momentum transports between phases depend on the interphase contact area. According to actual flow states, the mixture models are applied to the interfacial transfers between water and vapor and between gas and vapor. The free surface model is applied between gas and water. The Rayleigh-Plesset equation provides the basis for the mass sources' control of vapor generation and condensation.

The respective continuity equations for each phase are

$$\frac{\partial(\gamma_w \rho_w)}{\partial t} + \nabla \cdot (\gamma_w \rho_w U_w) = \dot{m}^- - \dot{m}^+$$
(1)

$$\frac{\partial(\gamma_{\nu}\rho_{\nu})}{\partial t} + \nabla \cdot (\gamma_{\nu}\rho_{\nu}U_{\nu}) = \dot{m}^{+} - \dot{m}^{-}$$
⁽²⁾

$$\frac{\partial(\gamma_g \rho_g)}{\partial t} + \nabla \cdot (\gamma_g \rho_g U_g) = 0$$
(3)

where γ , ρ and U are the volume fraction, density and velocity, respectively, \dot{m}^- and \dot{m}^+ are the mass transfer rates of condensation and vaporization, and subscripts w, v and g denote the water, vapor and gas phases, respectively.

The momentum equations for the three phases are

$$\frac{\partial(\gamma_{w}\rho_{w}U_{w})}{\partial t} + \nabla \cdot (\gamma_{w}(\rho_{w}U_{w} \otimes U_{w})) = -\gamma_{w}\nabla p_{w} + \nabla \cdot (\gamma_{w}\mu_{w}(\nabla U_{w} + (\nabla U_{w})^{T})) + (\Gamma_{wv}^{+}U_{v} - \Gamma_{vw}^{+}U_{w}) + \gamma_{w}\rho_{w}\mathbf{g} + M_{w}$$

$$(4)$$

$$\frac{\partial(\gamma_{\nu}\rho_{\nu}U_{\nu})}{\partial t} + \nabla \cdot (\gamma_{\nu}(\rho_{\nu}U_{\nu} \otimes U_{\nu})) = -\gamma_{\nu}\nabla p_{\nu} + \nabla \cdot (\gamma_{\nu}\mu_{\nu}(\nabla U_{\nu} + (\nabla U_{\nu})^{T})) + (\Gamma^{+}_{\nu\nu\nu}U_{w} - \Gamma^{+}_{w\nu}U_{\nu}) + \gamma_{\nu}\rho_{\nu}\mathbf{g} + M_{\nu}$$
(5)

$$\frac{\partial(\gamma_g \rho_g U_g)}{\partial t} + \nabla \cdot (\gamma_g (\rho_g U_g \otimes U_g)) = -\gamma_g \nabla p_g + \nabla \cdot (\gamma_g \mu_g (\nabla U_g + (\nabla U_g)^T)) + \gamma_g \rho_g g + M_g$$
(6)

where p and μ are the pressure and dynamic viscosity, respectively, $\Gamma_{\alpha\beta}^{+}U_{\beta} - \Gamma_{\beta\alpha}^{+}U_{\alpha}$ is the momentum transfer of phase α induced by the mass transfer between phases α and β , and g is the gravitational acceleration. M is the interfacial force due to the presence of other phases:

$$\boldsymbol{M}_{\alpha} = \sum_{\alpha \neq \beta} C_{dp} \rho_{\alpha\beta} A_{\alpha\beta} | \boldsymbol{U}_{\beta} - \boldsymbol{U}_{\alpha} | (\boldsymbol{U}_{\beta} - \boldsymbol{U}_{\alpha})$$
(7)

where M_{α} is the interfacial force acting on phase α , C_{dp} is the drag coefficient between two different phases, $\rho_{\alpha\beta}$ is the mixture density, $\rho_{\alpha\beta} = \gamma_{\alpha}\rho_{\alpha} + \gamma_{\beta}\rho_{\beta}$, $A_{\alpha\beta}$ is the interfacial area per unit volume, where $A_{\alpha\beta} = 2|\nabla\gamma_{\alpha}||\nabla\gamma_{\beta}|/(|\nabla\gamma_{\alpha}| + |\nabla\gamma_{\beta}|)$ for the free surface model and $A_{\alpha\beta} = \gamma_{\alpha}\gamma_{\beta}/d_{\alpha\beta}$ for the mixture model, and $d_{\alpha\beta}$ is the mixture length scale.

Combining the phase continuity equations with the constraint condition on the phase volume fractions, $\gamma_w + \gamma_v + \gamma_g = 1$, the volume conservation equation yields

$$\sum_{\alpha} \frac{1}{\rho_{\alpha}} \left(\frac{\partial(\gamma_{\alpha} \rho_{\alpha})}{\partial t} + \nabla \cdot (\gamma_{\alpha} \rho_{\alpha} \ U_{\alpha}) \right) = \sum_{\alpha} \frac{1}{\rho_{\alpha}} \left(S_{MS\alpha} + \sum_{\beta=1}^{N_{p}} \Gamma_{\alpha\beta} \right)$$
(8)

where $S_{MS\alpha}$ is the mass source of phase α , $\Gamma_{\alpha\beta}$ is the mass flow rate from phases β to α per unit volume, and N_p is the phase number.

To close the set of hydrodynamic equations, the constraints on pressure are given in the following form, whereby all of the phases share the same pressure field:

$$p_a = p, \ \alpha = 1, ..., N_p.$$
 (9)

2.2. Turbulence model

The shear stress transport (SST) model based on $k - \omega$ (Menter, 1994) accounts for the transport of the turbulent shear stress and gives reasonably good predictions of the onset and amounts of flow separation under adverse pressure gradients. The model is suitable for simulating ventilated supercavitating flows and for analyzing gas entrainment (Yu et al., 2010). The model uses the $k - \omega$ model in the near-wall region and the $k - \varepsilon$ model in the free-stream, i.e., it combines the best of the two models, where the ω -equation is different from that of the standard $k - \varepsilon$ model. Grids are clustered at the wall to guarantee a range of $0 < y^+ < 30$ for the separated flows when the SST model is used. Based on the grid spacing near the wall, the switch between a wall function formulation and a low-Reynolds number form is made.

$$\frac{\partial(\rho k)}{\partial t} + \nabla \cdot (\rho k U) = \nabla \cdot \left[\left(\mu + \frac{\mu_t}{\sigma_{k3}} \right) \nabla k \right] + P_k - \beta' \rho k \omega + P_{kb}$$
(10)

$$\frac{\partial(\rho\omega)}{\partial t} + \nabla \cdot (\rho\omega \boldsymbol{U}) = \nabla \cdot \left[\left(\mu + \frac{\mu_t}{\sigma_{\omega 3}} \right) \nabla \omega \right] + \alpha_3 \frac{\omega}{k} P_k - \beta_3 \rho \omega^2 + \frac{2\rho (1 - F_1)}{\sigma_{\omega 2} \omega} \nabla k \nabla \omega + P_{\omega b}$$
(11)

where μ_t is formulated as $\mu_t = \alpha_1 \rho k / \max(\alpha_1 \omega, SF_2)$. The model constants are obtained by weighting the two $k - \varepsilon$ and $k - \omega$ models (Owis and Nayfeh, 2003):

$$\phi = F_1 \phi_1 + (1 - F_1) \phi_2 \tag{12}$$

where ϕ_1 and ϕ_2 are the constants of the $k - \omega$ Wilcox model (Wilcox,

Download English Version:

https://daneshyari.com/en/article/8061852

Download Persian Version:

https://daneshyari.com/article/8061852

Daneshyari.com